Influence of shear flow on vesicles near a wall: A numerical study

Sreejith Sukumaran* and Udo Seifert[†]

Max-Planck-Institut für Kolloid- und Grenzflächenforschung, Am Mühlenberg 2, 14476 Golm, Germany

We describe the dynamics of three-dimensional fluid vesicles in steady shear flow in the vicinity of a wall. This is analyzed numerically at low Reynolds numbers using a boundary element method. The area-incompressible vesicle exhibits bending elasticity. Forces due to adhesion or gravity oppose the hydrodynamic lift force driving the vesicle away from a wall. We investigate three cases. First, a neutrally buoyant vesicle is placed in the vicinity of a wall that acts only as a geometrical constraint. We find that the lift velocity is linearly proportional to shear rate and decreases with increasing distance between the vesicle and the wall. Second, with a vesicle filled with a denser fluid, we find a stationary hovering state. We present an estimate of the viscous lift force that seems to agree with recent experiments of Lorz *et al.* [Europhys. Lett. **51**, 468 (2000)]. Third, if the wall exerts an additional adhesive force, we investigate the dynamical unbinding transition that occurs at an adhesion strength linearly proportional to the shear rate.

I. INTRODUCTION

We would like to understand how hydrodynamic flow affects vesicles and, in particular, shear flow because it occurs whenever a fluid flows near a surface. This is of relevance in modeling artificial or natural cells in motion from the level of the dynamics of a single cell to the rheology of a suspension such as the blood. It will also enable us to understand the interplay between vesicles in shear flow and specific and nonspecific adhesive properties of a membrane. This is a key feature in phenomena such as leukocyte locomotion [1,2]. Computational methods are now increasingly used to understand and analyze experiments studying the relationship between receptor-ligand functional properties and the dynamics of adhesion. An efficient numerical method simulating adhering spherical cells in flow has been used recently to investigate the physical kinetics of adhesion molecules [3]. There are compelling reasons to go beyond spherical cells, viz. (a) to understand how deformation couples with the dynamics of adhesion centers and (b) to study the interplay between the physical kinetics of adhesion molecules, orientation of a cell and viscous lift forces that act on nonspherical cells and do not act on spherical cells. It should, however, be noted that leukocyte locomotion is further complicated by the role of actin polymerization, ion channels, and pseudopod formation that together play an important role in leukocyte response to shear stress [4]. Another practical use of this study concerns mechanosensory transduction, which is the process by which certain cells convert fluid stresses to biochemical and/or electrical signals [5]. The identification and activation of mechanoreceptors and intracellular signaling pathways are currently active areas of research. For an example of a case where our study is relevant, consider an experiment that investigates the influence of mechanical stress on the activation of specific proteins present on the membrane of endothelial cells. One method involves reconstituting the proteins into phospholipid vesicles, which are then subjected to physiological levels of fluid shear stress in a viscometer [6]. Quantitative predictions require information regarding hydrodynamic stresses and tensions that develop in response to flow and the model discussed in this paper is suited for these purposes.

We are also motivated by recent experiments on weakly adhering vesicles in shear flow [7]. These investigations reveal the lipid flow within the vesicle membrane and the flow field within the vesicle and near its outer surface. The influence of weak flow fields on the state of adhesion and the translational motion of vesicles are studied using bright field and reflection interference contrast microscopy. Moreover, the hydrodynamic lift forces exerted on adhering vesicles are estimated and the lift forces are found significantly larger than estimates based on an earlier theoretical study [2]. An explanation for this discrepancy based on arguments using a lubrication analysis of flow between a spherical cap and a wall has been proposed recently [8].

Here, we show the results of a numerical simulation. With the above experiment in mind, we simulate an incompressible vesicle in shear flow, which is influenced by gravitational forces or nonspecific adhesion forces to be near a wall and by viscous lift forces to be away from the wall. The main objectives of this paper are (a) to understand the very nature of viscous lift force; (b) to describe how the steady state shape is influenced by shear flow and forces due to gravity or an adhesion potential; and (c) to study the influence of shear in taking the system away from equilibrium. The numerical method simulates a realistic model of a vesicle. The tensions that develop in response to flow are determined self-consistently.

Before describing the study, we take stock of what is known about the dynamics of vesicles, and about techniques that are relevant. The dynamics of vesicles belong to a broad class of problems called free-interface problems that describe the dynamics of a particle consisting of a membrane that encloses a drop of an incompressible Newtonian fluid often called a capsule in the literature [9]. The first problem discussed in this class was the behavior of a fluid drop in shear

———————
*Electronic address: sreesuku@hotmail.com
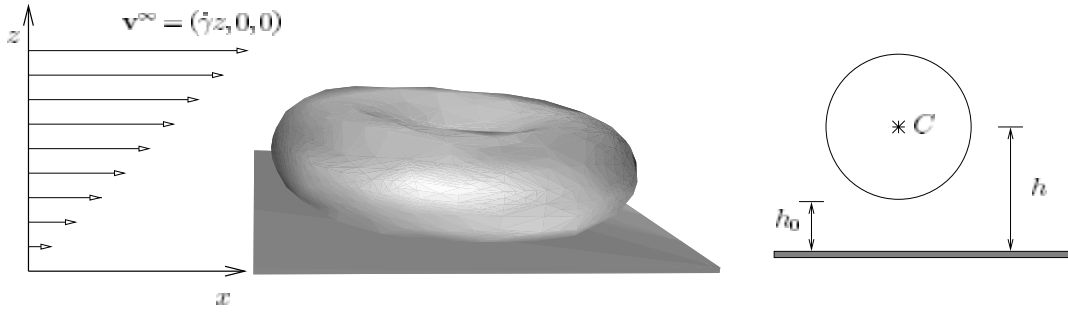
[†]Electronic address: useifert@mpikg-golm.mpg.de

FIG. 1. Schematic representation of the geometry showing a vesicle, the wall in the plane $z=0$, and applied linear shear flow. On extreme right, the mean center $(x_C, 0, z_C)$ is shown as C. The height of the center h and the vesicle-wall distance h_0 are also shown.

flow, when the effects of fluid viscosity and interfacial tension are taken into account [10]. In fact, much of the later work on elastic capsules or vesicles employed techniques and analysis used to understand the dynamics of liquid drops. The first two lines of attack involved analytical methods based on perturbation schemes for shapes close to a sphere, and theories using slender-body dynamics. Considerable effort has been made in fluid drop dynamics ranging from drop breakup to physical influences such as surfactants and complex flows, for reviews see [11,12]. An important step in understanding this nonlinear problem of three-dimensional deformation in external flows without making drastic approximations involves numerical methods using boundary element methods [13]. The use of an unstructured grid of triangular elements to represent the interface has been shown to be efficient and numerically stable in simulating the dynamics of three-dimensional liquid droplets in shear flow in an unbounded fluid and in the proximity of a bounding plane wall [14]. This has been also used in simulating capsules with elastic membranes [15]. We now compare this scene of activity with that regarding the dynamics of vesicles.

In the last three decades, experimental and theoretical studies of the behavior of free and bound fluid vesicles in equilibrium have met with great success [16]. But, the hydrodynamics of vesicles still poses unsolved problems. For example, consider a vesicle in unbounded shear flow. A minimal model of a vesicle involves bending elasticity and the constraints of fixed area and volume. Using this model, the dynamics of free vesicles in shear flow have been studied using boundary element methods [18,19]. Apart from features similar to liquid drops such as steady revolution of the surface, called tank treading in the case of capsules, and a steady tilt, the numerical work suggested that shear is a singular perturbation even though one would naively expect that at very small shear rates the equilibrium shape is recovered. Numerical limitation prevented a conclusive examination of this regime.

In *two dimensions*, the dynamics of adhering vesicles has been investigated in models for chemotaxis [20] and in shear flow [21] using a boundary element method. Practical considerations and a need to compare theoretical models with experiments call for an investigation of how hydrodynamic flows affect *three-dimensional* vesicles.

In the next section, the physical model of a vesicle and the

mathematical formulation of the hydrodynamics of vesicles including the implementation of the boundary element method will be briefly discussed. Then, we proceed to three sections concerning the dynamics of vesicles in shear flow in the proximity of a wall. In Sec. III, we study the nature of viscous hydrodynamic lift force and we assume that the vesicle does not experience gravitational force, i.e., the vesicle is neutrally buoyant, and the vesicle is not influenced by forces due to an adhesion potential. In Sec. IV, gravitational forces are introduced and we compare our results with the experiment. In Sec. V, the influence of a nonspecific adhesion potential is considered. And in Sec. VI, our conclusions regarding the dynamics of vesicles near a wall are summarized.

II. MODEL

Consider the vesicle to be a two-dimensional surface embedded in three-dimensional space. The instantaneous membrane configuration $\mathbf{R}(s_1, s_2)$ is parametrized by internal coordinates (s_1, s_2). The energy E of the vesicle—with an area element dS—

$$E \equiv \oint dS \left[\frac{\kappa}{2} (2H)^2 + \Sigma + \mathcal{W} \right], \tag{1}$$

has three contributions. The first due to the squared mean curvature H^2 describes the bending energy [16] with bending rigidity κ. The second term is due to a locally varying isotropic tension Σ that is needed to ensure local incompressibility of the membrane. The third term is the adhesion energy due to the proximity of a homogeneous substrate that exerts a nonspecific interaction. The geometry is schematically represented in Fig. 1. The adhesion potential, with the wall in the plane $z=0$, is chosen to be

$$\mathcal{W}(z) \equiv W(d_0/z)^2 [(d_0/z)^2 - 2]. \tag{2}$$

Here, W is the adhesion strength. The potential is repulsive as $1/z^4$ for $z \ll d_0$ and attractive as $-1/z^2$ at long distance. The potential has a minimum of $-W$ at $z=d_0$. Theoretically, any model with a strongly repulsive short range interaction and a weakly attractive long range interaction would be suitable. Numerically, the model chosen is most suitable because it minimizes numerical problems associated with sharply di-

verging forces at short length scales. In any specific physical situation, the exact form of the potential depends nonuniversally on the concrete experimental conditions (see review, [17]). As long as this potential is repulsive on short length scales and attractive on long length scales, with a single minimum in between, the results derived in the present study will hold, at least qualitatively. In the case of free vesicles, the adhesion term is absent. The membrane force density **f** reads

$$\mathbf{f}(\mathbf{R}) \equiv -\left(\frac{1}{\sqrt{g}} \frac{\delta E}{\delta \mathbf{R}} \right), \tag{3}$$

where g is the determinant of the metric tensor.

To describe the hydrodynamics of vesicles, we assume that the Reynolds number of the flow inside and around the vesicle based upon the vesicle size (say the radius of the spherical vesicle of equal volume) is sufficiently small so that the velocity **v** of the fluid and the pressure field p is governed by the equations of Stokes flow or creeping flow equations. Thus

$$\eta^{out} \partial_{jj} v_i^{out} = \partial_i p^{out}, \quad \partial_i v_i^{out} = 0,$$
$$\eta^{in} \partial_{jj} v_i^{in} = \partial_i p^{in}, \quad \partial_i v_i^{in} = 0, \tag{4}$$

where p^{out} and p^{in} are the pressures, and η^{out} and η^{in} are the viscosities associated with the outer and inner fluids, respectively, and ∂_i denotes differentiation with respect to the coordinate $x_i = x, y, z$ for $i = 1, 2, 3$, respectively. The summation convention is used over doubly occurring indices.

If the vesicle is not neutrally buoyant, then we account for the body force acting on the vesicle due to gravity. This is done by modifying the membrane force density. The modified force density $\mathbf{f}^{mod}$ is given by [13]

$$\mathbf{f}^{mod}(\mathbf{R}) = \mathbf{f}(\mathbf{R}) + (\rho^{in} - \rho^{out})(\mathbf{g} \cdot \mathbf{R})\mathbf{n}(\mathbf{R}). \tag{5}$$

Here, ρ^{in} and ρ^{out} are the densities of the outer and inner fluids, respectively; **n** is the unit vector normal to the vesicle, $\mathbf{g} \equiv -g_0 \hat{\mathbf{e}}_z$ is the acceleration due to gravity where $g_0 \simeq 9.81 \text{ m s}^{-2}$ and $\hat{\mathbf{e}}_z$ is the unit vector in the z direction.

To express the no-slip condition on bounding surfaces and also the impermeability of the membrane, we require that the velocity be continuous across the vesicle. This also provides the kinematic condition by which the vesicle shape changes with time. The hydrodynamic surface force is allowed to undergo a discontinuity that is balanced by the membrane forces, $\mathbf{f}^{mod}(\mathbf{R})$.

Rather than solve for the fluid velocity at all points in space, it is advantageous to use a boundary-integral method by which the Stokes equations inside and outside are cast into an integral form that involves only quantities evaluated on the vesicle surface [13]. This formalism provides us with an integral equation for the membrane velocity in terms of **f**,

$$v_i(\mathbf{R}^\alpha) = v_i^\infty(\mathbf{R}^\alpha) + \frac{1}{8\pi\eta} \oint G_{ij}(\mathbf{R}^\alpha, \mathbf{R}^\beta) f_j(\mathbf{R}^\beta) dS, \tag{6}$$

where $\mathbf{v}^\infty(x, y, z) = (\dot{\gamma}z, 0, 0)$ is the incident shear flow (refer Fig. 1) and $G_{ij}(\mathbf{R}^\alpha, \mathbf{R}^\beta)$ is the appropriate Green's function for the velocity. In the case of free vesicles in unbounded space, the free-space Green's function is the Stokeslet; and, in the case of bound vesicles, we choose the semi-infinite space Green's function for the velocity [22,23]. We emphasize that the internal and external fluid flow can also be computed self-consistently using this formalism. This formalism includes, of course, the modification of the external flow due to the presence of the dynamically evolving vesicle. To make computations tractable, we assume that the viscosity of the fluid inside the vesicle is equal to that of the suspending fluid, ($\eta^{out} = \eta^{in} = \eta$). If the viscosities are different, equation (6) is modified to include an additional term that turns it into an integral equation in **v**. Then, the equation has to be solved iteratively or **v** must be determined by matrix inversion at any instant of time. We also note in passing that by choosing the same viscosity, we do not allow for tumbling motion in shear flow that occurs when the dynamics is vorticity dominated. For liquid drops, tumbling is shown to occur for $\lambda \equiv \eta^{in}/\eta^{out} \geq 4$ [14].

We characterize vesicles by a dimensionless number, the reduced volume

$$v \equiv V/(4\pi R_0^3/3), \tag{7}$$

where V is the enclosed volume and the surface area A determines the length scale $R_0 = \sqrt{A/(4\pi)}$. For a sphere, $v = 1$. The bending rigidity of the membrane κ sets the energy scale. We do not incorporate thermal fluctuations. Throughout this paper, unless otherwise mentioned, lengths are expressed in units of R_0, the adhesion strength in units of κ/R_0^2, and the shear rate in units of $\kappa/(8\pi\eta R_0^3)$. When gravitational forces are considered, the dimensionless gravity parameter

$$g' \equiv (\rho^{in} - \rho^{out})g_0 R_0^4/\kappa \tag{8}$$

measures this effect. In simulations involving the adhesion potential equation (2), we take $d_0 = 0.01R_0$. This restriction is used to minimize numerical problems associated with sharply diverging forces at short length scales. For a 1 μm vesicle, this would place the minimum at a reasonable value of 10 nm. For larger vesicles, the choice $d_0 = 0.01R_0$ puts the minimum somewhat too far from the wall. However, numerical restrictions prevented us from using an even smaller d_0: R_0 ratio.

The implementation of the boundary element method is now well established [14,15,18,19]. Here, we briefly mention the essential steps.

(a) The surface is approximated by a grid of triangular elements. We take 512 triangles with 258 nodes.

(b) The force density is calculated at the nodes.

(c) Along with the condition dictated by two-dimensional incompressibility,

$$\frac{\partial}{\partial t} \sqrt{g} = \partial_i v_i - n_i n_j \partial_j v_i = 0, \tag{9}$$
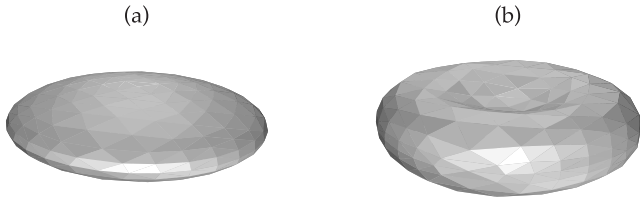
(a)   (b)

FIG. 2. An example of a test of the numerical method in which an initial shape relaxes to a stationary shape known to exist in the absence of externally applied flow. (a) The initial shape is chosen to be an oblate convex spheroid with reduced volume, $v=0.6$. (b) After relaxation, the equilibrium or stationary shape is a stable oblate biconcave discocyte with the initial area and volume.

the integral equation Eq. (6) yield equations for the local tensions Σ. Unlike droplets with constant tension, the tensions Σ develop so that the membrane element deforms while maintaining the original area.

(d) After computing Σ, the integral equation (6) is solved for **v**.

(e) The positions of the nodes are advanced, the coordinates updated, and we return to step (b) unless a steady state is reached. If one is interested in computing external or internal flow fields at any instant, it can be easily done with an additional step in the algorithm, in which equation (6) is modified by replacing R_α by **r**, where **r** is the coordinate of an external or an internal point.

Before tackling cases involving externally imposed hydrodynamic flows, we test if the numerical scheme yields the stationary shapes that are known to exist in equilibrium conditions, i.e., neutrally buoyant free vesicles [16]. The minimal model we have chosen allows a wide spectrum of shapes. For $0.65 \lesssim v \lesssim 1$, the stable states are prolatelike spheroids. For $v \lesssim 0.75$, oblate discocytes are locally stable. So far, there is no indication of the presence of locally stable nonaxisymmetric shapes in this model. For $\mathbf{v}^\infty = \mathbf{0}$, our numerical scheme gives the stable and metastable axisymmetric shapes, including dumb-bell shaped prolates and erythrocytelike biconcave discocytes. In Fig. 2, we show an example in which the initial oblate spheroid relaxes to the final equilibrium (stationary) biconcave shape. Within this minimal model, the vesicle relaxes to the next dynamically accessible

locally stable shape. Depending on the initial condition, this is a prolate, an oblate, or a stomatocyte.

In contrast to vesicles, the shape of *incompressible* interfaces that are not influenced by curvature elasticity is infinitely degenerate. In such cases, the stationary shape depends only upon the membrane surface area, and as a consequence of neglecting elastic behavior, the interface can retain any shape with the same surface area. At the other end of the spectrum, liquid drops with interfaces influenced by a constant surface tension and also compressible interfaces that are only influenced by curvature elasticity remain spherical.

III. UNBOUND NEUTRALLY BUOYANT VESICLES NEAR A WALL

We now simulate the influence of steady shear flow on vesicles in the proximity of a wall. To retrieve the bare contribution of hydrodynamics to the lift force, adhesion and gravity are not considered in this section. The vesicle is initially at a small distance from the wall and then, shear flow is imposed. In Fig. 3, a typical sequence of ''snapshots'' are shown. In the far field, the vesicle translates with a speed of the same order of the difference of velocity, due to external shear flow, that exists across the vesicle. The vesicle also experiences a lift velocity. From Fig. 3, it can be extracted that the lift velocity is an order of magnitude smaller than the translational velocity.

Analyzing several cases, we find the main characteristics in this setup to be: (i) the membrane of the vesicle tank treads; (ii) the vesicle develops a steady tilt, which is roughly independent of the shear rate; and (iii) the shape changes to a prolatelike ellipsoid. This is similar to the dynamics of a free vesicle in unbounded shear flow [18]. The first two features are understood [24,26]. The tank-treading motion is due to the rotational component of linear shear flow. The balance of the moments on the vesicle due to the effect of shear-flow acting on a stationary inclined vesicle and that due to the tank-treading motion results in a steady tilt. These two moments are linearly proportional to shear rate and hence, the tilt is independent of the shear rate in the steady state. In the case of liquid droplets, the tilt reduces more drastically with shear rate because of the elongation of the droplet, and
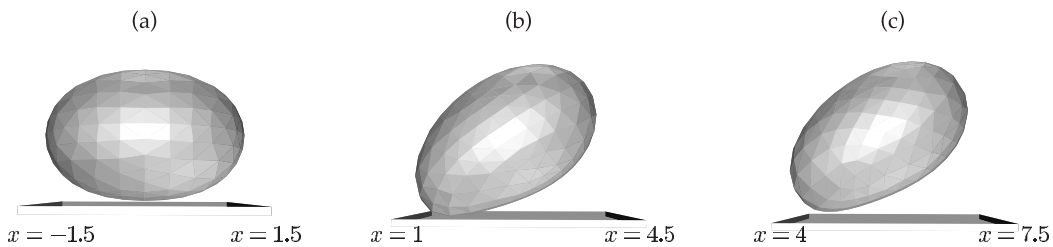
(a)   (b)   (c)

$x=-1.5$ $x=1.5$ $x=1$ $x=4.5$ $x=4$ $x=7.5$

FIG. 3. ''Snapshots'' of the liftoff of an unbound vesicle away from a wall in the presence of shear flow. The plane $z=0$ shown is the wall. The x coordinate at the end points of the wall is shown at each instance of time t. Here, $v=0.95$, $\dot{\gamma}=30$. (a) At $t=0$, the initial shape is an oblatelike spheroid. The vesicle is at a distance $h_0=0.1R_0$. (b) The shape is now a prolatelike ellipsoid and the vesicle is tilted with respect to the shear plane. Here, $t=0.075$. (c) The shape and tilt of the vesicle is roughly the same as before, and the liftoff is now clearly seen at $t=1.5$. All quantities are given in dimensionless units as discussed in the text.
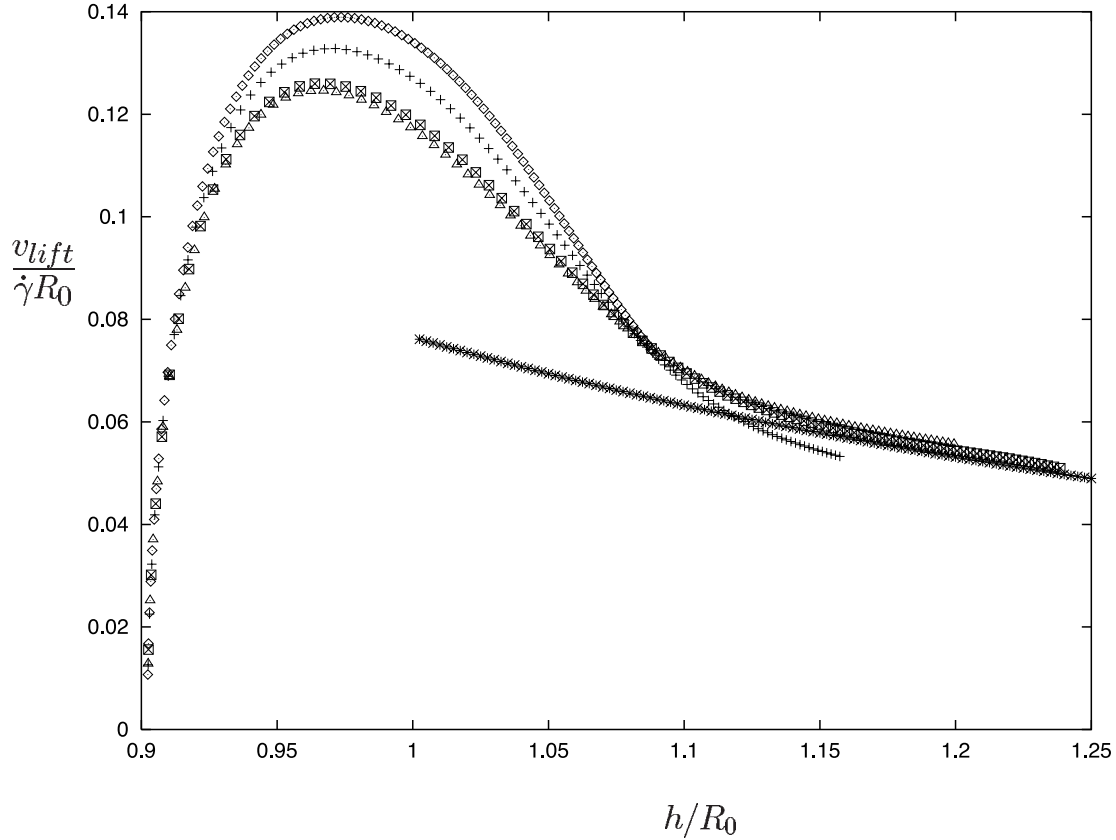
FIG. 4. The ratio of mean lift velocity v_{lift} to shear rate times the radius of vesicle $\dot{\gamma}R_0$ is plotted against the ratio of the mean height h of the vesicle from the wall to the the radius of vesicle for different shear rates (definitions are given in the text). The lift velocity of the vesicle is roughly proportional to the shear rate. Here, $v=0.95$, and in dimensionless units, $\dot{\gamma}=6$ ($\diamond$), 10 ($+$), 30 ($\square$), 50 ($\times$) and the estimated asymptotic fit given by Eq. (10) is plotted using the asterisk ($*$).

thereby a reduction in v. But in the case of vesicles considered here, v is a constant due to incompressibility. As mentioned in the introduction, for the third feature regarding the prolate ellipsoidal shape, it is still not understood whether it will persist for arbitrarily small shear rates.

From the above discussion, it is clear that the steady tilt of the vesicle plays the leading role in breaking the fore-aft symmetry of the vesicle with respect to shear flow. Since the tilt is independent of shear rate, the excess pressure in the space between the vesicle and the wall can be expected to cause a lift force that is proportional to shear rate $\dot{\gamma}$. In fact, the dynamics of a vesicle near a nonadhering wall is roughly similar for any shear rate; and as a function of $\tau \equiv \dot{\gamma}t$, the "snapshots" as shown in Fig. 3 will be similar for vesicles with the same reduced volume. In Fig. 4, we plot for different shear rates the ratio of lift velocity v_{lift} to shear rate against the mean height. The data collapse indicates that $v_{lift} \propto \dot{\gamma}$.

We now derive an empirical expression for the lift velocity guided by the far-field result obtained for ellipsoidal cells: $v_{lift} = U\dot{\gamma}(R_0^3/h^2)$ where $U \simeq 0.1-0.3$ for $v \simeq 0.9-0.99$ [25]. Assuming the same power law, we get an estimated asymptotic fit for the lift velocity to be

$$v_{lift} \simeq 0.08\dot{\gamma}\frac{R_0^3}{h^2} \quad (v=0.95). \quad (10)$$

Here, h is the mean distance of the center of the vesicle to the substrate. We have simply calculated the mean center and the mean velocity to be the arithmetical mean of the coordinates and velocity of the nodes, respectively. Then, v_{lift} is just the vertical or z component of the mean velocity. The fit needs to be taken with caution due to three reasons. First, the exact dependence of v_{lift} on h is not easy to access with the limited range as shown in Fig. 4. Second, the asymptotic fit (and also, far-field results based on analytical methods) for vesicle migration assumes that the problem can be treated in a quasistatic way. This implies that it is strictly valid only when the time scale for deformation and shape changes is much smaller than the time scale for migration. Since our numerical method is similar to an experimental situation and we do not arbitrarily fix the position of a vesicle, the fit is probably valid only for large shear rates. This is partially evident from Fig. 4 where we see that the plots for lower shear rates do not exactly collapse onto the plots for higher shear rates. Third, there is no reason to expect asymptotic results to hold good for $h \simeq 0.25-0.5R_0$. But, there is also no reason to be alarmed if it is true in that range. In fact, analogous results
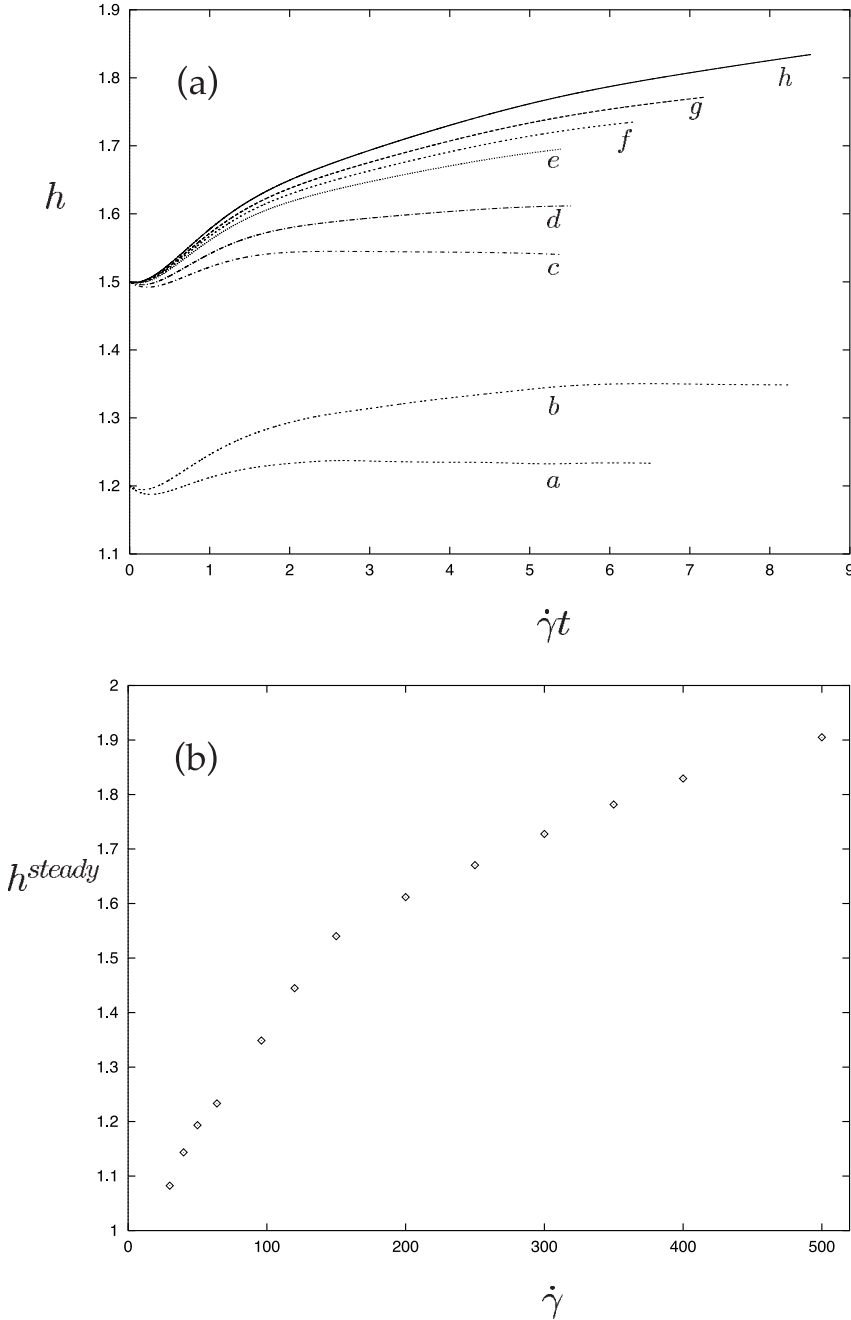
FIG. 5. (a) Mean vertical height of the vesicle h versus $\dot{\gamma}t$ for different shear rates. The shear rates $\dot{\gamma}$ are (a) 64, (b) 96, (c) 150, (d) 200, (e) 300, (f) 350, (g) 400, and (h) 500. (b) Steady state height of the vesicle h versus the shear rate, $\dot{\gamma}$. Here, $v = 0.95$, $g' = 6.4$, and $\dot{\gamma}$ is given in dimensionless units as described in the text.

for liquid drops do indeed match remarkably well for $\lambda = 1$ at $h \simeq 0.25 - 0.5 R_0$ [15]. We can also infer from far-field results that the sign of the prefactor is determined by the sign of the tilt θ of the vesicle. Hence, when $\dot{\gamma} \rightarrow -\dot{\gamma}$ and $\theta \rightarrow -\theta$, $v_{lift} \rightarrow v_{lift}$, which agrees with expectations that the direction of migration should be independent of the direction of shear flow.

We emphasize that the dominant effect is due to the tilt of the vesicle and this leads to a lift force $F_{lift} \propto \dot{\gamma}$. Additional effects due to deformation can be expected to be of $O(\dot{\gamma}^2)$.

For $h \simeq R_0$, the asymptotic lift velocity can be taken to be the lower bound for the lift velocity. The actual velocity could be expected to be higher due to transient effects or due the effect of "touching" the wall. Assuming Stokes' result

$6\pi\eta R_0 v_{lift}$, this lower bound for the viscous lift force can be estimated from Eq. (10) for $v = 0.95$ to be

$$F_{lift} \simeq 0.45 \pi \eta \dot{\gamma} \frac{R_0^4}{h^2}. \tag{11}$$

With this estimate of the lift force, a comparison can be made with the results of the experiment. We shall do so only at the end of the next section, after investigating the influence of gravity.

IV. INFLUENCE OF GRAVITY

The effect of gravity on vesicles arises from the frequently employed experimental technique to stabilize the
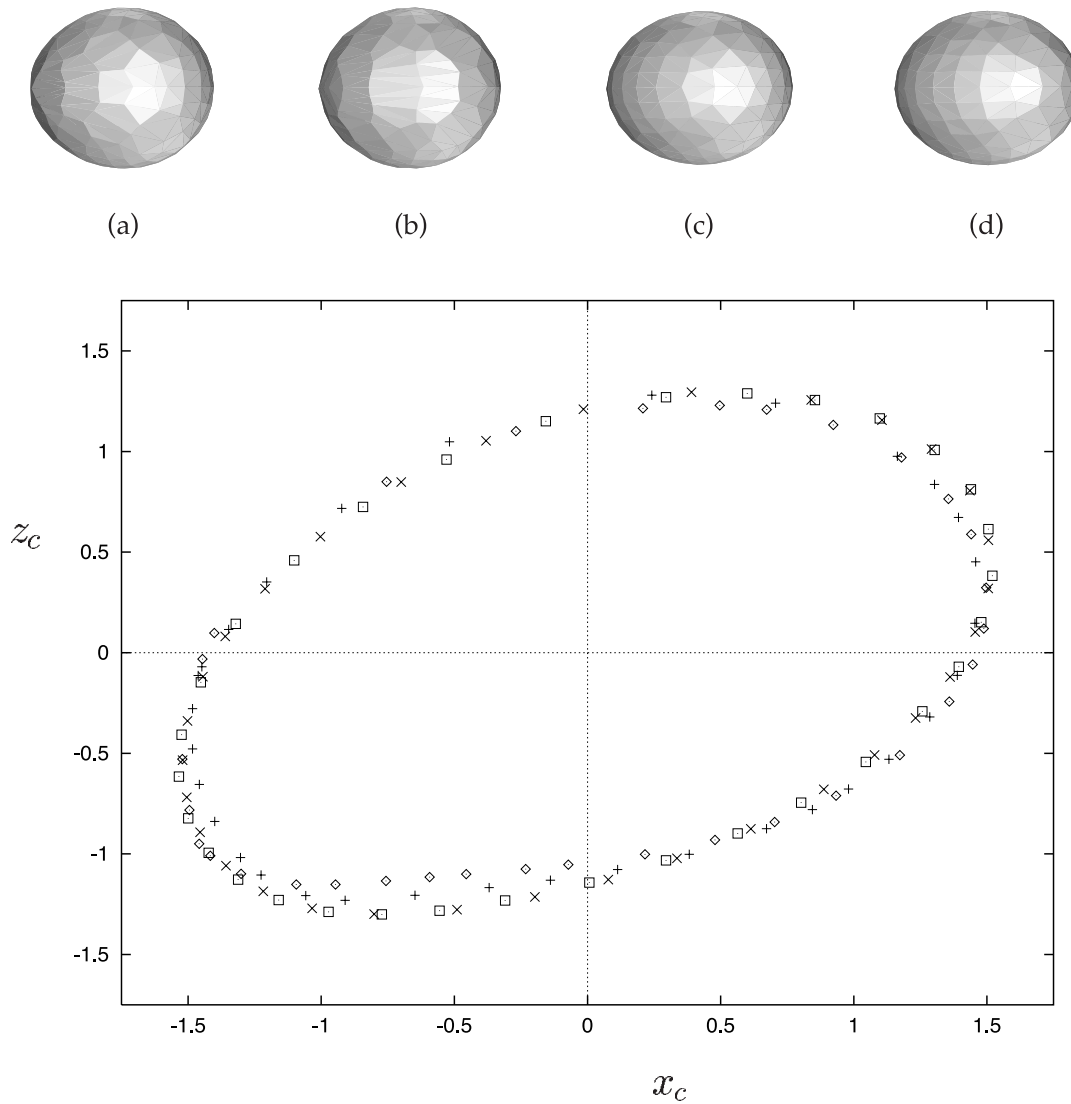
FIG. 6. The profile of a vesicle in the $x-z$ plane and the top view (looking down z axis) are shown for four different shear rates (in dimensionless units). (a) $\dot{\gamma}=64$ ($\diamond$), (b) $\dot{\gamma}=96$ ($+$), (c) $\dot{\gamma}=350$ ($\times$) and (d) $\dot{\gamma}=400$ ($\square$). The profile is shown on axes x_c-z_c such that their mean centers coincide. Here, $v=0.95$ and $g'=6.4$.

vesicle at the bottom of the measurement chamber by a difference in density between the fluids inside and outside the vesicle. In the experiment [7], this is done by choosing iso-osmolar but different buffers for swelling the vesicle and suspending the vesicle. The threshold velocity at which unbinding of the vesicle from the substrate occurs allows to estimate the lift force. After unbinding, the vesicle hovers at a distance at which electrostatic forces or van der Waals forces that cause adhesion are negligible. The lift force in the hovering state can therefore be assumed to be counteracted by gravitational forces only.

We simulate the influence of gravitational force on a vesicle. As in the previous section, we place the vesicle initially at a distance $h_0 \simeq 0.1R_0 - 0.5R_0$ and then, shear flow is applied. It would of course be more realistic if we started with a vesicle that rested on the wall, but at gravitational strengths, which are of relevance, this initial configuration leads to numerical instabilities. Instead, the initial h_0 is al-

lowed to be nonzero but we check if the steady state dynamics is independent of h_0 and the simulations confirm this view. We note in passing that the steady state depends on the reduced volume of the vesicle but does not depend on the initial shape.

As expected, gravity counteracts viscous lift force and the vesicle hovers at a distance away from the wall. We now study how this distance depends on the shear rate. It is clear from Fig. 5(a) that the initial h_0 can be chosen so that we can optimize the computational time in evolving the vesicle to the steady state. At large shear rates, the vesicle is sufficiently far from the wall and as discussed in the previous section, the lift is determined by the tilt alone. Meanwhile, at low shear rates, the vesicle is also deformed by the proximity to the wall. The dependence of the steady state mean height on shear rate is shown in Fig. 5(b) and seems to indicate those two regimes.

Let us now consider the three-dimensional shape of the

vesicle in the steady state. In Fig. 6, we show a comparison of the profile and also the top view of the vesicle for different shear rates. We note the features that are immediately apparent from Fig. 6.

(i) Vesicles with small excess areas $v \rightarrow 1$ do not exhibit large deformations with increasing shear rate.

(ii) At large shear rates [refer Figs. 6(c) and 6(d)], the shape of the vesicle is roughly independent of shear rate.

(iii) At any shear rate, the part of the vesicle away from the wall shows roughly the same inclination.

(iv) At lower shear rates [refer Figs. 6(a) and 6(b)], gravity reduces the vesicle-wall distance. To allow for greater contact area, the shape changes from a prolatelike to an oblatelike ellipsoid.

(v) The tilt of the contact area decreases with decreasing shear rate. There is no unique definition of this tilt and therefore, the tilt of the "base" is difficult to quantify.

Now, we compare our results with the experiment [7]. There are some problems in making this comparison. The reduced volume v and the gravitational strength g' are not exactly known. For vesicles with very small excess area, the experiment does not report any measurable tilt of the contact area nor the overall shape. Such a picture fits in with our description only in the limit $g' \rightarrow \infty$. We take the shape of the vesicle to be close to a sphere with $v = 0.95$. We assume the values quoted, viz. the density difference, $\rho^{in} - \rho^{out} \simeq 5.2$ mg/ml, the radius of the vesicle $R_0 \simeq 14$ μm, the vesicle-wall gap $h_0 \simeq 100$ nm and shear stresses typically $\eta \dot{\gamma} \simeq 1.2$ mPa. These experimental values lead to an estimated gravitational force on a vesicle with volume V of

$$F_{grav} = (\rho^{in} - \rho^{out}) g_0 V \simeq 6 \times 10^{-13} \text{ N}. \quad (12)$$

As a theoretical estimate, we obtain the lift force based on Eq. (11) assuming that $h \simeq R_0$ as

$$F_{lift} \simeq 0.45 \pi \eta \dot{\gamma} R_0^2 \simeq 3 \times 10^{-13} \text{ N}. \quad (13)$$

The agreement should be taken with a grain of salt if one takes into consideration all the assumptions that have gone into these estimates.

V. INFLUENCE OF ADHESION

Now, we consider the dynamics of vesicles adhering to a surface due to nonspecific interactions. Here, the interplay between forces due to an adhesion potential, Eq. (2), and hydrodynamic forces is considered. The vesicle is assumed to be neutrally buoyant.

Like an experiment, we start with an adhering vesicle, then apply shear flow and watch how the vesicle responds. The dynamical evolution in the transient stage is shown in Fig. 7. These "snapshots" are qualitatively similar for any adhering vesicle with arbitrary reduced volume at any adhesion strength or shear rate. The tilting of the vesicle is similar to the scenario in the preceeding section.

The steady state of the adhering vesicle, of course, depends on the reduced volume, adhesion strength and shear rate. Unlike the case involving gravity, vesicles adhering to a substrate by the influence of a short range potential cannot be
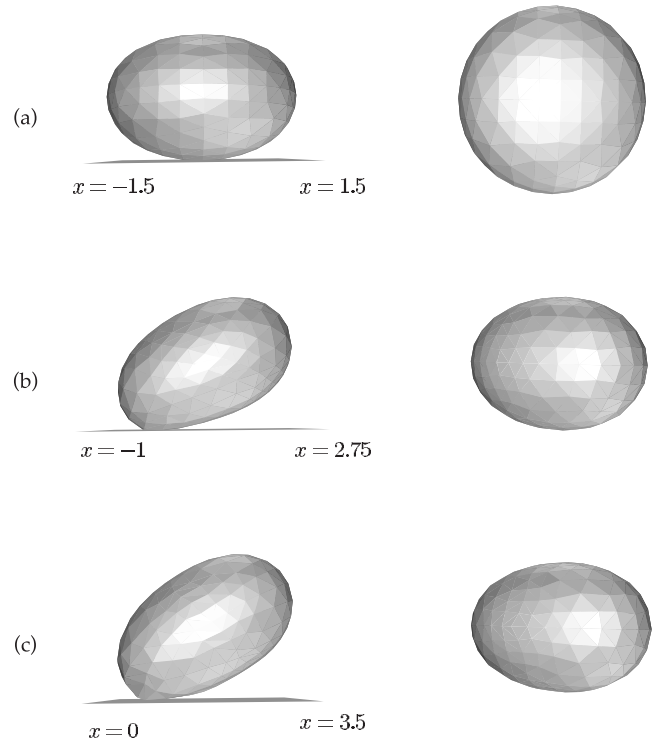

FIG. 7. The dynamical evolution of an adhering vesicle is shown. Here, $v = 0.95$, $\dot{\gamma} = 2$, and $W = 0.1$ (all quantities scaled to be dimensionless as described in the text). The top and side views are shown on the right side and left side, respectively. (a) An adhering vesicle in equilibrium resembles an oblate spheroid at $t = 0$. (b) In the transient stage the shape changes to a tilted prolatelike ellipsoid, ($t = 0.6$). (c) In the steady state, $t = 1.2$, the tank-treading vesicle is "pinned" to the wall and slips/rolls along the wall. The wall in the plane $z = 0$ is in the side view. The x coordinate at the end points of the wall is shown at each instance of time.

made to hover at any arbitrary height by tuning the strength of adhesion. There is a critical shear rate above which the vesicle unbinds from the wall. For smaller shear rates, the vesicle tank treads along the substrate. In Fig. 8, we show how the critical shear rate varies with increasing adhesion strength for a vesicle with reduced volume, $v = 0.95$. For $\dot{\gamma} \lesssim \dot{\gamma}_c$, the steady state shape of the vesicle resembles the shape shown in Fig. 7(c). Two main features of this state are to be noted. One, the tilt of the vesicle is nearly the same as that of a nonadhering vesicle near a wall, and not very different from the tilt of a free vesicle in shear flow. Two, the surface of adhesion is nearly zero. The vesicle can be said to be "pinned." This state is nearly similar for any adhesion strength and this explains the roughly linear relationship between the critical shear rate $\dot{\gamma}_c$ and the adhesion strength. For lower shear rates or higher adhesion strengths, the area of contact increases and a typical example of a "bound" steady state is shown in Fig. 9. We find that the process of unbinding, viz. "bound" $\rightarrow$ "pinned" $\rightarrow$ unbound or "free," is similar to that described with simulations of the two-dimensional model [21].

Finally, we summarize the results of the simulations with a dynamical phase diagram. First, we recall the behavior of
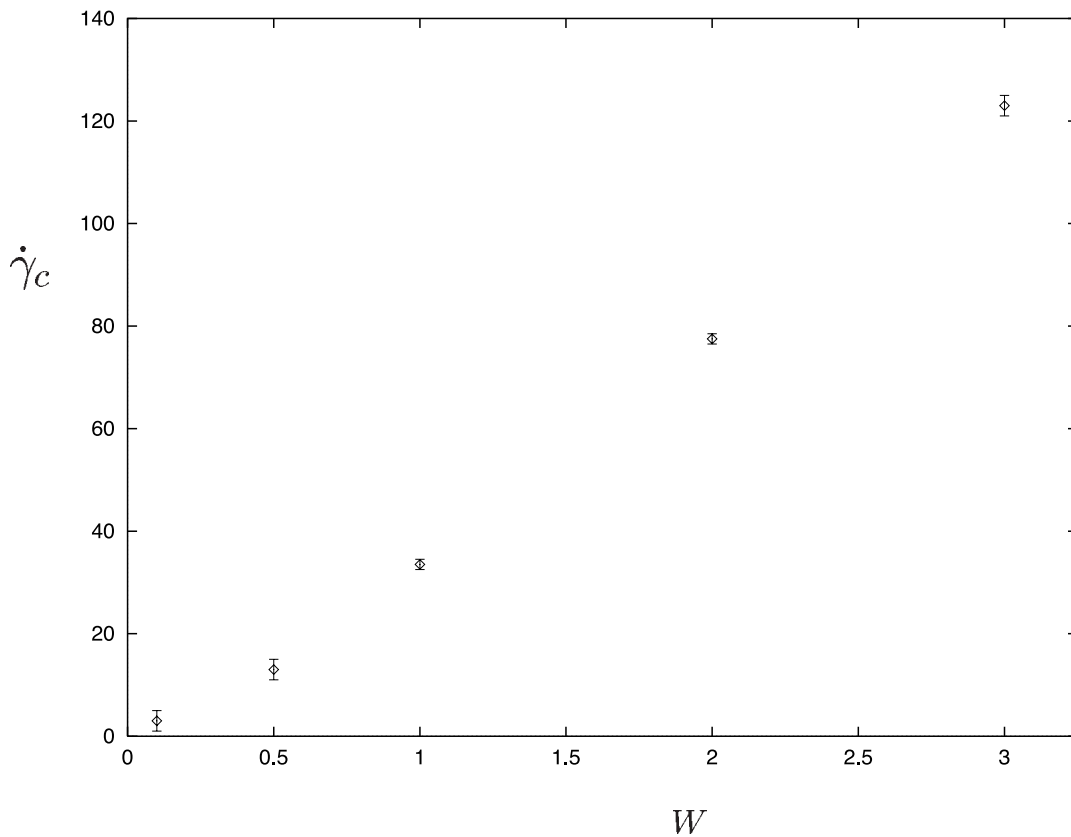
FIG. 8. The critical shear for unbinding $\dot{\gamma}_c$ is plotted against the adhesion strength W for $v = 0.95$, and $\dot{\gamma}_c$ is linearly proportional to the adhesion strength W. Here, $d_0 = 0.006$. With $\kappa = 10^{-19}$ J, $\eta = 10^{-3}$ J s/m^3, $R_0 = 5$ μm, and with W roughly $10^{-10} - 3 \times 10^{-9}$ J/m^2, the critical shear rate is roughly in the range $0.1 - 4$ s^{-1}.

adhering vesicles under equilibrium conditions. In the absence of shear, it is known that there are two states [16]. For weak adhesion, the shape of the vesicle resembles the free shape and the surface of adhesion is zero. This state is called the pinned state. It should, however, be noted that there is no unique definition of the pinned state in the dynamical picture. When adhesion is strong, there is the bound state with nonzero adhesion area. The adhesion area also depends on the excess area, which is a measure of the reduced volume. For $0.5 < v < 1$, the transition from the bound axisymmetric shape to the pinned state is discontinuous. Keeping in mind the similarity between the equilibrium and dynamical situations, we can construct a schematic dynamical phase diagram (refer Fig. 10). Apart from the two-stage dynamical unbinding, we expect in the limit of weak adhesion, a regime in which the unbinding goes through only one stage. In the case

of an adhesion potential with finite range, there will be a finite critical shear rate for unbinding a vesicle that is pinned under equilibrium conditions. If the vesicle is pinned by a contact potential, the vesicle will unbind for any shear rate. This regime is difficult to realize either numerically or ex-
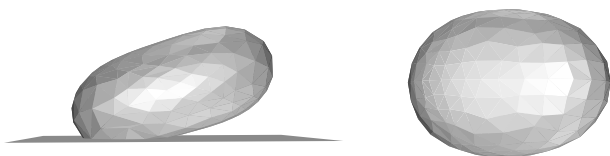

FIG. 9. An example of a ''bound'' state. Here, $v = 0.87$, $\dot{\gamma} = 2$, $W = 0.2$ (in dimensionless units as described in the text). The side and top view are shown on the left side and right side, respectively.
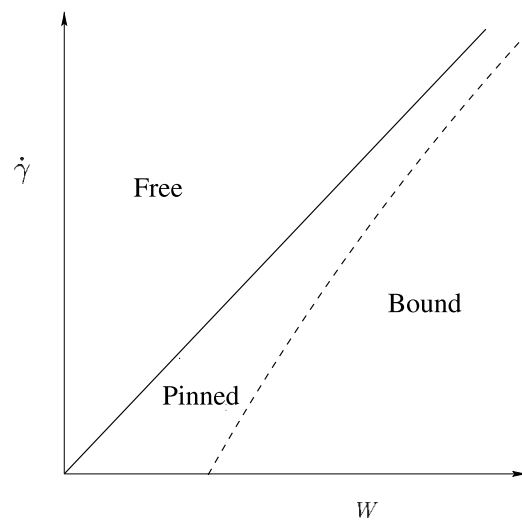

FIG. 10. Schematic phase diagram in the shear rate $\dot{\gamma}$, adhesion strength W plane with free, pinned, and bound shapes for vesicles with arbitrary area and volume.

perimentally. In principle, there could be a direct transition between bound and free vesicles but we have not found any evidence for it based on the numerical simulations over a wide range of parameters.

VI. CONCLUSION

We conclude this study of the dynamics of vesicles near a wall with observations regarding the computation, summary of main results, and certain remarks about current limitations and ongoing research. Using the boundary element method with a grid of triangular elements, we are able to simulate incompressible vesicles in bounded and unbounded shear flow. With moderate shear rates, adhesion, and gravitation strengths, the numerical method is stable and effective in studying the steady state of adhering, hovering or free vesicles. The algorithm, which is used to ensure area incompressibility, is the main hurdle in improving the speed of computation and also in using finer discretization.

We are able to find the following features regarding the nature of viscous lift force on incompressible vesicles with bending elasticity.

(i) The lift force due to the tilt of the vesicle is linearly proportional to the shear rate. It is the dominant part in our simulations also for small shear rates.

(ii) Our numerical results agree well with a recent experiment.

(iii) The general features of dynamical unbinding is similar to that in simulations of the two-dimensional model even though the additional possibility of a prolate-oblate shape change complicates the issue.

We also remark about interesting issues that need to be resolved, both experimentally and theoretically. We have only considered a situation where the viscosities of the inside and outside fluid are equal. This is definitely an oversimplification of experiments with cells though it is not a limitation for experiments with phospholipid vesicles. We still have to understand whether the model considered is singular in the limit of very small shear rates. We have not done simulations with the ratio of vesicle-wall gap to radius, $h_0/R_0 < 0.001$. In this limit of vanishing gap, features such as the roughness of the wall and also, the no-slip boundary condition will have to be reassessed. Finally, we note that the numerical method discussed here is amenable to an extension that includes specific receptor-ligand type of adhesion.

[1] P. Bongrand, Rep. Prog. Phys. **62**, 921 (1999).

[2] R. Bruinsma, in *Physics of Biomaterials, Fluctuations, Self Assembly and Evolution*, Vol. 332 NATO Advanced Studies Institute Series E: Applied Science, edited by T. Risk and D. Sherrington (Kluwer, Dodrecht, 1996).

[3] Kai-Chien Chang, D.F.J. Tees, and D.A. Hammer, Proc. Natl. Acad. Sci. U.S.A. **97**, 11262 (2000).

[4] F. Moazzam, F.A. DeLano, B.W. Zweifach, and G.W. Schmid-Schönbein, Proc. Natl. Acad. Sci. U.S.A. **94**, 5338 (1997).

[5] P.F. Davies, Physiol. Rev. **75**, 519 (1995).

[6] S. Gudi, J.P. Nolan, and J.A. Frangos, Proc. Natl. Acad. Sci. U.S.A. **95**, 2515 (1998).

[7] B. Lorz, R. Simson, J. Nardi, and E. Sackmann, Europhys. Lett. **51**, 468 (2000).

[8] U. Seifert, Phys. Rev. Lett. **83**, 876 (1999). Note that in the last term in Eq. (14) of this reference, a factor $(R/R_a)^4$ is missing arising from the correct conversion of W to Σ.

[9] D. Barthés-Biesel, J. Fluid Mech. **100**, 831 (1980).

[10] G.I. Taylor, Proc. R. Soc. London, Ser. A **146**, 501 (1934).

[11] J.M. Rallison, Annu. Rev. Fluid Mech. **16**, 45 (1984).

[12] H.A. Stone, Annu. Rev. Fluid Mech. **26**, 65 (1994).

[13] C. Pozrikidis, *Boundary Integral and Singularity Methods for Linearized Viscous Flow* (Cambridge University Press, Cambridge, England, 1992).

[14] M.R. Kennedy, C. Pozrikidis, and R. Skalak, Comput. Fluids **23**, 251 (1994).

[15] S. Ramanujan and C. Pozrikidis, J. Fluid Mech. **361**, 117 (1998).

[16] U. Seifert, Adv. Phys. **46**, 13 (1997), and references therein.

[17] R. Lipowsky and E. Sackmann, *Structure and Dynamics of Membranes*, Handbook of Biological Physics, Vols. 1A and 1B (Elsevier Science, Amsterdam, 1995).

[18] M. Kraus, W. Wintz, U. Seifert, and R. Lipowsky, Phys. Rev. Lett. **77**, 3685 (1996).

[19] M. Kraus, Ph.D. thesis, Universität Potsdam, 1996 (unpublished).

[20] I. Cantat and C. Misbah, Phys. Rev. Lett. **83**, 235 (1999).

[21] I. Cantat and C. Misbah, Phys. Rev. Lett. **83**, 880 (1999).

[22] The free space Green's function (*Stokeslet* or *Oseen-Burgers tensor*) is

$$G_{ij}(\mathbf{x},\mathbf{x}_0) \equiv G_{ij}^0(\mathbf{x},\mathbf{x}_0) = \frac{\delta_{ij}}{r} + \frac{\hat{x}_i \hat{x}_j}{r^3},$$

where $\hat{\mathbf{x}} = \mathbf{x} - \mathbf{x}_0$, $r = |\hat{\mathbf{x}}|$ and δ_{ij} is the delta function. The Green's function for flow bounded by a plane wall is given by [23]

$$G_{ij}(\mathbf{x},\mathbf{x}_0) = G_{ij}^0(\hat{\mathbf{x}}) - G_{ij}^0(\hat{\mathbf{X}}) + 2b_0^2 G_{ij}^D(\hat{\mathbf{X}}) - 2b_0 G_{ij}^{SD}(\hat{\mathbf{X}}),$$

where the wall is located at $z = w$, $b_0 = z_0 - w$, $\hat{\mathbf{X}} = \mathbf{x} - \mathbf{x}_0^{IM}$ and $\mathbf{x}_0^{IM} = (x_0, y_0, 2w - z_0)$ is the image of $\mathbf{x}_0$ with respect to the wall. The matrices G_{ij}^D and G_{ij}^{SD} are

$$G_{ij}^D(\mathbf{x}) = \pm \left(\frac{\delta_{ij}}{|\mathbf{x}|^3} - 3 \frac{x_i x_j}{|\mathbf{x}|^5} \right),$$

$$G_{ij}^{SD}(\mathbf{x}) = x_3 G_{ij}^D(\mathbf{x}) \pm \frac{\delta_{j3} x_i - \delta_{i3} x_j}{|\mathbf{x}|^3},$$

with a minus sign for $j = 3$, corresponding to the z direction, and a plus sign for $j = 1,2$, corresponding to the x and y directions.

[23] J.R. Blake, Proc. Cambridge Philos. Soc. **70**, 303 (1971).

[24] For the sake of completeness, we note that it was pointed out [25] that the tank-treading frequency ω and the steady tilt θ as computed for this model show remarkable agreement with a

very different model, in the spheroidal limit, which has an analytical solution [26]. This exactly solvable model consists of a tank-treading ellipsoidal membrane with fixed shape and the boundary condition on the cell surface is that the velocity be a generic linear function of the coordinates. The analytical results are: the tilt is given by, $\cos 2\theta = (l_3^2 - l_1^2)/(l_3^2 + l_1^2)$, and the

rotational frequency $\omega = (l_1/l_3)/(1 + (l_1/l_3)^2)$, in units mentioned before. Here, l_1 and l_3 are the short axis and the long axis, respectively.

[25] P. Olla, J. Phys. II **7**, 1533 (1997).
[26] S.R. Keller and R. Skalak, J. Fluid Mech. **120**, 27 (1982).